Particle-in-cell simulation with Vlasov ions and drift kinetic electrons

Yang Chen and Scott E. Parker
University of Colorado at Boulder, Boulder, Colorado 80309, USA

(Received 9 January 2009; accepted 27 April 2009; published online 20 May 2009)

There are certain limitations in using gyrokinetic ions for simulations of turbulent transport in tokamak plasmas. Applications where Vlasov ions might be more appropriate include the electron temperature gradient driven turbulence, edge turbulence with steep density gradient, and magnetic reconnection in a weak guide field. In such cases the ion gyrokinetic model presently used in simulations needs to be extended, but a satisfactory extension valid for fully electromagnetic turbulence is not presently available. Even if an accurate model is found, its numerical implementation could be very challenging. We propose a kinetic model that combines Vlasov ions with gyrokinetic electrons to avoid the difficulties with gyrokinetic ions. The field equations of this model are the Faraday's equation and the Ampere's equation without the displacement current. The perturbed fields $\mathbf{B}_1$ and $\mathbf{E}_1$ rather than the scalar and vector potentials are used to formulate the field equations. We have devised an implicit scheme for this model, demonstrated in three-dimensional slab for the Alfvén waves, the drift Alfvén instability and the ion acoustic waves. © *2009 American Institute of Physics*. [DOI: 10.1063/1.3138743]

I. INTRODUCTION

Present kinetic simulations of anomalous transport due to ion-Larmor-radius scale fluctuations in fusion plasmas are based on the gyrokinetic model for ions. In this paper we attempt to return to the conventional particle-in-cell (PIC) simulation based on the ion Vlasov equation. This is motivated by the following considerations. First, the gyrokinetic formalism is based on a number of assumptions (the gyrokinetic ordering). For instance, the parameter $\varepsilon_B=\rho_i/L_B$ (ρ_i is the ion Larmor radius and L_B is the scale length of the equilibrium field variation) is a fundamental gyrokinetic ordering parameter. For small devices such as the National Spherical Torus Experiment (NSTX) $\varepsilon_B\sim 0.1$ for the energetic ions. Belova *et al.*[1] showed that for such devices the lowest-order magnetic moment $\mu_0=mv_\perp^2/2B$ used in current gyrokinetic simulations as a constant of motion can vary by as much as 50% along the equilibrium particle trajectories. Other ordering assumptions can also become questionable. In the plasma edge pedestal the scale length of the equilibrium density and temperature profiles are not much larger than the ion Larmor radius (e.g., $\varepsilon=\rho_i/L_n\geq 0.1$, L_n is the edge pedestal density scale length). In the transport barrier there is often present a strong $\mathbf{E}\times\mathbf{B}$ flow comparable to the ion thermal speed. In both situations the ion gyrokinetic model presently used needs to be extended. The theoretical formulation of electrostatic gyrokinetic model appropriate for core transport barriers is itself nontrivial.[2] A geometrically generalized Vlasov–Maxwell system of equations that is valid for edge plasmas has been derived by Qin *et al.*,[3] but the field equations in terms of the distribution function of the guiding center variables are not explicitly provided, and no attempt is made to separate the compressional Alfvén waves from the shear Alfvén waves, as is typically done in the current gyrokinetic simulations. Without the guide of prior experience it is not clear at all how a numerical implementation of the generalized Vlasov–Maxwell equations should proceed. Second, the main constraint on efficient gyrokinetic simulation with kinetic electrons is due to the fast electron motion along the magnetic field line. This motion is not eliminated in the gyrokinetic model. In practice we found that for small devices such as NSTX a time step of $\Omega_i\Delta t=0.2$ has to be used for numerical stability in GEM (Ref. 4) simulations. With a time step slightly smaller it appears possible to follow the ion gyromotion accurately while using the same drift kinetic model for the electrons.

The Vlasov equation is appealing to PIC implementation for its formal simplicity. It has not been used in turbulent simulations partly due to the need to resolve the gyromotion in comparison with gyrokinetic model and partly due to the presence of high frequency modes in the model. However, many high frequency modes can be eliminated readily. By using a quasineutral field equation, e.g., dropping the displacement term in the Ampere's equation, plasma oscillations are eliminated. For the electrons the same drift kinetic equation can be used, which eliminates the electron cyclotron scale. It turns out that for modes with $k_\theta\rho_i\sim 1$, the compressional Alfvén mode poses the most severe constrain on the time step. Implicit method is necessary for overcoming this constraint.

In Sec. II we describe the Vlasov ion/drift kinetic electron model. An implicit δf scheme is presented in Sec. III, which is demonstrated for the Alfvén waves, the electron temperature gradient (ETG) driven drift Alfvén instability, and the ion acoustic waves (IAWs) in Sec. IV. Section V contains more discussions on the rationale of developing this hybrid simulation model. In the Appendix a gyrokinetic extension of the model for the electrons is described.

II. EQUATIONS FOR VLASOV ION/DRIFT KINETIC ELECTRON SIMULATION

In gyrokinetic simulations one of Maxwell's equations takes the form of quasineutrality condition (the gyrokinetic Poisson equation),[5] in which the ion polarization density explicitly depends on the electric potential, much like the space

charge term in the original Poisson equation. This feature is lost once the ions are treated fully kinetically. We therefore use the Faraday's law and the Ampere's equation

$$\frac{\partial \mathbf{B}_1}{\partial t} = -\nabla \times \mathbf{E}_1, \tag{1}$$

$$\nabla \times \mathbf{B}_1 = \mu_0(\mathbf{J}_i + en_e\mathbf{V}_e), \tag{2}$$

where $\mathbf{J}_i$ and $\mathbf{V}_e$ are the perturbed ion current and electron flow velocity, respectively. The subscript 1 denotes perturbed quantities. By dropping the displacement term in the Ampere's equation, quasineutrality is implied. Since ions are described by the Vlasov equation, $\mathbf{J}_i$ is obtained from the particle ions directly. The electrons are described by the drift kinetic equation

$$\frac{\partial f_e}{\partial t} + \mathbf{v}_G \cdot \nabla f_e + \dot{\varepsilon}\frac{\partial f_e}{\partial \varepsilon} = 0, \tag{3}$$

the guiding center velocity is given by

$$\mathbf{v}_G = v_\parallel \tilde{\mathbf{b}} + \mathbf{v}_D + \mathbf{v}_E, \tag{4}$$

where $\tilde{\mathbf{b}} = \mathbf{b} + \mathbf{B}_{\perp 1}/B_0$ and $\mathbf{b}$ is the unit vector along the equilibrium magnetic field $\mathbf{B}_0$, $\mathbf{v}_D$ is the grad-B and curvature drift, and $\mathbf{v}_E$ is the $\mathbf{E}\times\mathbf{B}$ drift. We have omitted the collisional term in Eq. (3). The rate of change of the particle kinetic energy $\varepsilon = (1/2)m_e v^2$ is

$$\dot{\varepsilon} = -e\mathbf{v}_G \cdot \mathbf{E}_1 + \mu\frac{\partial B_{\parallel 1}}{\partial t}. \tag{5}$$

In a guiding center model, the flow $\mathbf{V}_e$ in Eq. (2) is given by

$$n_e\mathbf{V}_e = \frac{n_e}{B_0}\mathbf{E}_1 \times \mathbf{b} - \frac{1}{eB_0}\mathbf{b} \times \nabla \delta p_{\perp e} + n_e U_{\parallel e}\mathbf{b}. \tag{6}$$

The first term is the guiding center current due to the $\mathbf{E}\times\mathbf{B}$ drift, the second is the diamagnetic flow associated with the perturbed perpendicular electron pressure

$$\delta p_{\perp e} = \int f_{e1}\mu B_0 d\mathbf{v}, \tag{7}$$

and the last term $n_e U_{\parallel e}$ is the parallel flow

$$n_e U_{\parallel e} = \int f_{e1} v_\parallel d\mathbf{v}. \tag{8}$$

In Eqs. (4) and (6) $B_0(\mathbf{x})$ is the magnitude of the equilibrium magnetic field. The amplitude of magnetic fluctuation in a tokamak plasma is typically small, $\delta B/B \leq 10^{-3}$, and its effect on the guiding center drift can be neglected. On the other hand, the electron density n_e in Eq. (6) is the total (equilibrium plus perturbation) density. This nonlinearity could be important in plasma edges since a large fluctuation $\delta n_e/n_e \sim 0.1$ is possible.

Equations (1), (2), and (6) are the field equations for the Vlasov ion/drift kinetic electron model. If a gyrokinetic model is used for the electrons, the electron flow should be replaced by the gyrokinetic result. The electron flow, Eq. (6), is appropriate only for drift kinetic electrons. A general expression with finite-Larmor-radius corrections can be obtained by applying the pull-back transformation to the velocity moment of the electron Vlasov distribution in gyrokinetic theory.[6,7] In general the gyrokinetic result for $k_\perp \rho_e \sim 1$ (ρ_e is the electron Larmor radius) with full electromagnetic effects is rather complicated and is expressed in terms of the electrostatic potential ϕ and the vector potential $\mathbf{A}$. In the Appendix we describe how to convert the Frieman–Chen nonlinear gyrokinetic equation[8] into a form which only employs $\mathbf{E}_1$ and $\mathbf{B}_1$, and how the electron current is to be computed. We note that the gyrokinetic electron model should be used exclusively for ρ_e scale fluctuations such as ETG turbulence. Once the electrons are treated as gyrokinetic, the gyrokinetic ordering must be obeyed, so that the nonlinearity contained in Eq. (6) due to the perturbed electron density $\delta n_e = n_e - n_{e0}$ must be dropped for consistency. In the following we will limit to drift kinetic electrons.

Guiding center electrons have been used with Vlasov ions in the HIDENEK code.[9] Our model differs from that of HIDENEK in that we have dropped the displacement term in the Ampere's equation, making the model explicitly quasineutral. Another major difference is numerical. We will develop the simulation algorithm primarily for the δf method, since for turbulent transport in tokamak plasmas it is a well-proven technique for reducing the particle noise.

Recently Lin *et al.*[10] used gyrokinetic electrons with Vlasov ions for the study of magnetic reconnection. Our approach differs from that of Lin *et al.* in the field model. Whereas we use $\mathbf{E}_1$ and $\mathbf{B}_1$ for both ions and electrons, Lin *et al.* only advance the ions with $\mathbf{E}_1$ and $\mathbf{B}_1$, the electrons being advanced with the electric potential ϕ and the vector potential $\mathbf{A}$ with ϕ obtained from the quasineutrality equation. By neglecting the displacement current the quasineutrality condition is implicit in our model, but it is not used as a field equation.

For simulation it is convenient to cast the Ampere's equation into the generalized Ohm's law for the electric field. Taking the time derivative of the Ampere's equation and combining it with the Faraday's equation yields

$$-\nabla \times \nabla \times \mathbf{E}_1 = \mu_0\left(\frac{\partial}{\partial t}\mathbf{J}_i + e\frac{\partial}{\partial t}(n_e\mathbf{V}_e)\right). \tag{9}$$

The parallel Ohm's law is obtained by taking the parallel component of this equation and combining it with the electron equation of motion

$$en_e\tilde{\mathbf{b}} \cdot \mathbf{E}_1 + \frac{m_e}{\mu_0 e}\mathbf{b} \cdot \nabla \times \nabla \times \mathbf{E}_1 = -\nabla \cdot \int m_e v_\parallel \mathbf{v}_G f_e d^3\mathbf{v} - \int \mu\tilde{\mathbf{b}} \cdot \nabla B_0 f_e d^3\mathbf{v}. \tag{10}$$

The ion contribution has been neglected because it is $\sim m_e/m_i$ smaller than the electron contribution, but see Sec. IV C for the importance of ion terms in simulations of IAWs.

The remaining two components of the Ampere's equation, Eq. (2), can be written as the perpendicular Ohm's law,

$$en_e\mathbf{E}_{\perp 1} = -\nabla_\perp \delta p_{\perp e} - \frac{B_0}{\mu_0}\mathbf{b}\times(\nabla\times\mathbf{B}_1) + \mathbf{B}_0\times\mathbf{J}_i. \quad (11)$$

The second term on the left hand side (lhs) of Eq. (10) comes from the inertia term in the electron equation of motion. Similar electron inertia term does not appear in Eq. (11) because the higher order electron polarization drift is neglected. We note that if Vlasov electrons are used the complete Ohm's law, in which the electron inertia effects appear also in the perpendicular direction, has to be used for consistency. Barnes *et al.*[11] recently proposed such a model. They also explored the algorithms for solving the Ohm's law, Eqs. (11) and (10), with massless fluid electron closure for the electron pressure.

III. IMPLICIT *δf* SCHEME FOR THE HYBRID KINETIC MODEL

In present gyrokinetic simulations Eqs. (1) and (2) are never solved for $\mathbf{E}_1$ and $\mathbf{B}_1$. Instead the perturbed fields are represented as $\mathbf{E}_1 = -\nabla\phi - (\partial A_\parallel/\partial t)\mathbf{b}$ and $\mathbf{B}_{1\perp} = \nabla\times A_\parallel\mathbf{b}$. The compressional Alfvén waves are thus eliminated. For ion-Larmor-radius scale fluctuations $k_\perp\rho_i \sim 1$ in low-β plasmas, the compressional waves have frequencies $\omega \gg \omega_{ci}$, posing the most severe constraint on the time step. It is essential to overcome this numerical difficulty. For practical applications in the foreseeable future we would also like to solve this problem in a δf PIC method. In this section we present an implicit δf scheme. The scheme is demonstrated in Sec. IV for the long wavelength Alfvén waves in a uniform plasma and the short wavelength drift Alfvén instability driven unstable by the ETG.

For demonstrative purpose we restrict the discussion to three-dimensional shearless slab geometry. We define $\beta_e = \mu_0 n_0 T_e/B_0^2$, the sound speed $c_s^2 = T_e/m_i$, and $\rho_s = m_i c_s/eB_0$. We normalize length with ρ_s and time with $\omega_{ci}^{-1} = m_i/eB_0$. In a shearless slab the linearized Ohm's equations, Eqs. (10) and (11), become in dimensionless form

$$E_{1\parallel} + \frac{m_e}{\beta_e m_i}\mathbf{b}\cdot\nabla\times\nabla\times\mathbf{E}_1 = -\nabla_\parallel \delta p_{\parallel e} - \mathbf{B}_{1\perp}\cdot\nabla p_{\perp e}, \quad (12)$$

$$\mathbf{E}_{1\perp} + \frac{1}{\beta_e}\mathbf{B}_0\times(\nabla\times\mathbf{B}_1) = -\nabla_\perp \delta p_{\perp e} - \mathbf{J}_i\times\mathbf{B}_0. \quad (13)$$

In Eq. (12) $p_{\perp e} = \int m_e v_\perp^2 f_{e0} d\mathbf{v}$ is the equilibrium pressure. Notice that due to the assumed slab geometry the second term on the right-hand side (rhs) of Eq. (10) vanishes. Both terms on the rhs of Eq. (12) are contained in the first term on the rhs of Eq. (10).

In the δf method the perturbed ion distribution function f_{i1} evolves along the trajectory according to

$$\frac{d}{dt}f_{i1} = -\frac{q}{m_i}(\mathbf{E}_1 + \mathbf{v}\times\mathbf{B}_1)\cdot\frac{\partial}{\partial\mathbf{v}}f_{i0}. \quad (14)$$

Equation (14) is valid for any equilibrium distribution f_{i0}. Unlike in the case of gyrokinetic ions, an instability drive term (the ω^* term) that is proportional to spatial gradient of f_{i0} does not appear explicitly in the f_{i1} equation. Such drive enters the weight equation implicitly through the velocity dependence of f_{i0}. For instance, in a uniform magnetic field the particle's parallel velocity $v_\parallel$, perpendicular velocity $v_\perp$, and the guiding center position $\eta = x + mv_y/qB_0$ are constants of motion, hence $f_{i0} = f_{i0}(v_\perp, v_\parallel, \eta)$,

$$\frac{\partial f_{i0}}{\partial\mathbf{v}} = \frac{\partial f_{i0}}{\partial v_\perp}\frac{\mathbf{v}_\perp}{v_\perp} + \frac{\partial f_{i0}}{\partial v_\parallel}\mathbf{b} + \frac{m}{qB_0}\frac{\partial f_{i0}}{\partial\eta}\hat{\mathbf{y}}. \quad (15)$$

The instability drive due to density or temperature gradient in the x-direction would then enter through the last term. In the following we assume the ion distribution to be a uniform Maxwellian with temperature T_i. If particles are loaded according to f_{i0}, then the ion weight evolves according to

$$\frac{d}{dt}w_i = -\frac{q}{T_i}\mathbf{E}_1\cdot\mathbf{v}. \quad (16)$$

Similarly the electron weight evolves according to

$$\frac{d}{dt}w_e = \kappa\left(v_{Ex} + v_\parallel\frac{B_{1x}}{B_0}\right) - \frac{e}{T_e}\mathbf{E}_1\cdot\mathbf{v}_G, \quad (17)$$

where $\kappa = \kappa_T(m_e v^2/2 - 3/2)$ and

$$\kappa_T = -\frac{1}{T_e}\frac{\partial T_e}{\partial x}.$$

The electron temperature is assumed to be nonuniform in the x-direction.

In the implicit scheme we treat the Faraday's equation, Eq. (1), and the perpendicular electric terms in the ion weight equation $q\mathbf{E}_{1\perp}\cdot\mathbf{v}_\perp$ implicitly. This leads to the following discretized form of the field equations:

$$\frac{\mathbf{B}_1^{n+1} - \mathbf{B}_1^n}{\Delta t} = -\nabla\times\mathbf{E}_1^{n+1}, \quad (18)$$

$$\mathbf{E}_{1\perp}^{n+1} + \frac{1}{\beta_e}\mathbf{B}_0\times(\nabla\times\mathbf{B}_1^{n+1}) = -\nabla_\perp\delta p_{\perp e}^{n+1} - \mathbf{J}_{i\perp}^{n+1}\times\mathbf{b}, \quad (19)$$

$$E_{1\parallel}^{n+1} + \frac{m_e}{m_i}\frac{1}{\beta_e}\mathbf{b}\cdot\nabla\times\nabla\times\mathbf{E}_1^{n+1} = -\nabla_\parallel\delta p_{\parallel e}^{n+1} - \mathbf{B}_1^{n+1}\cdot\nabla p_{\perp e}. \quad (20)$$

Here the superscript indicates the time step.

In Eq. (19) the ion current $\mathbf{J}_{i\perp}^{n+1}$ depends on the unknown $\mathbf{E}_{1\perp}^{n+1}$. We first advance the ion weight from w_j^n to w_j^* with $E_{1\parallel}^n$ and use this intermediate weight to compute an intermediate current $\mathbf{J}_{i\perp}^*$,

$$w_j^* = w_j^n + \frac{q}{T_i}\delta E_\parallel^n v_\parallel \Delta t, \quad (21)$$

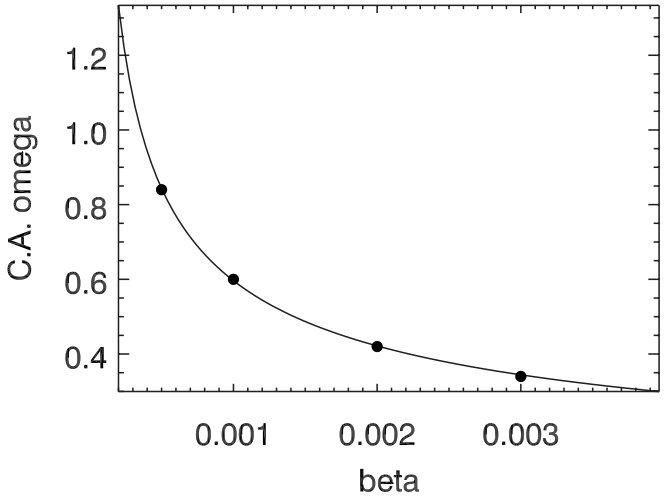

FIG. 1. Simulated Compressional Alfvén wave frequencies vs β_e (points) compared with the dispersion relation (solid line).

$$\mathbf{J}_{i\perp}^{*} = q\frac{V}{N}\sum_j \frac{1}{\Delta V} w_j^{*}\mathbf{v}_{\perp j} S(\mathbf{x}-\mathbf{x}_j^{n+1}). \tag{22}$$

Here S is the linear interpolation function for deposition, V is the plasma volume, N is the number of particles, and $\Delta V = \Delta x \Delta y \Delta z$. Notice that in Eq. (22) the particle position at the future time step is used. The dependence of $\mathbf{J}_{i\perp}^{n+1}$ on the unknown $\mathbf{E}_1^{n+1}$ comes from the increment to particle weight from $\mathbf{E}_{1\perp}^{n+1}$,

$$\begin{aligned}\mathbf{J}_{\perp i}^{n+1}(\mathbf{x}) &= \mathbf{J}_{i\perp}^{*}(\mathbf{x}) + \Delta t\frac{V}{N}\sum_j \frac{1}{\Delta V}\frac{q}{T_i} \\ &\quad \times \mathbf{v}_\perp \mathbf{E}_{1\perp}^{n+1}(\mathbf{x}_j^{n+1})\cdot \mathbf{v}_j^{n+1} S(\mathbf{x}-\mathbf{x}_j^{n+1}) \\ &\approx \mathbf{J}_{\perp i}^{*}(\mathbf{x}) + qn_{i0}\Delta t \mathbf{E}_{1\perp}^{n+1}(\mathbf{x}) \\ &\equiv \mathbf{J}'_{\perp i},\end{aligned} \tag{23}$$

where the second equation follows because the marker distribution is a Maxwellian. After the field equations are solved, the ion weight is updated from w_j^{*} to w_j^{n+1},

$$w_j^{n+1} = w_j^{*} + \frac{q}{T_i}\mathbf{E}_{1\perp}^{n+1}\cdot \mathbf{v}_\perp \Delta t. \tag{24}$$

We find that replacing $\mathbf{J}_{\perp i}^{n+1}(\mathbf{x})$ with $\mathbf{J}'_{\perp i}(\mathbf{x})$ does not lead to observable difference in the following simulations. If the difference is important, Eq. (19) can be solved iteratively, treating the difference between $\mathbf{J}_{\perp i}(\mathbf{x})$ and $\mathbf{J}'_{\perp i}(\mathbf{x})$ as a small perturbation.

Equations (19) and (20) can be solved using the Fourier transform method. Once $\mathbf{E}_1^{n+1}$ is available, $\mathbf{B}_1^{n+1}$ is advanced according to Eq. (18).

In Sec. IV example simulations are presented. We end this section with a comment on recovering the electrostatic model from our field equations. Drift wave turbulence in toroidal plasmas is frequently studied in the electrostatic limit with "electromagnetic" effects added separately. With the $A_\parallel/\phi$ field model this separation of the electrostatic and electromagnetic effects can be conveniently done by treating the parallel Ampere's equation for $A_\parallel$ as optional. Thus the electrostatic turbulence is studied by only solving the quasineutrality condition for ϕ while setting $A_\parallel = 0$. This is equivalent to setting $\beta_e = 0$ since in dimensionless form the Ampere's equation for $A_\parallel$ is[12]

$$-\nabla_\perp^2 A_\parallel = \beta_e j_\parallel. \tag{25}$$

This convenient feature is lost in the field model presented here. Equations (19) and (20) become singular at $\beta_e = 0$, hence it cannot be used to determine $\mathbf{E}_1$ in the electrostatic limit. It is always possible to define the electrostatic limit by setting $\mathbf{B}_1 = 0$ and enforcing quasineutrality, which implicitly determines $\mathbf{E}_1$. But this requires an algorithm very different from the implicit scheme presented here.

IV. EXAMPLES OF SIMULATIONS

In this section the implicit δf scheme is applied to the simulation of Alfvén waves, drift Alfvén instabilities, and the IAWs. In all the simulations an ion-to-electron mass ratio of $m_i/m_e = 1837$ is used.

A. Shear and compressional Alfvén waves

The previous implicit scheme is intended to eliminate the fast compressional Alfvén waves on the $k_\perp \rho_i \sim 1$ scale. On the longer scale $k_\perp \rho_i \ll 1$, the fast wave frequency given by $\omega = k v_A$, where $v_A = \mu_0 n_i m_i / B_0^2$ is the Alfvén velocity, is below the ion cyclotron frequency and well resolved by a time step $\omega_{ci}\Delta t \ll 1$. This is shown in Fig. 1 for the $k_\perp \rho_s = 0.019$, $k_\parallel = 0$ mode. The simulations are initialized with a finite $B_{1\parallel}$. The time step is $\omega_{ci}\Delta t = 0.05$.

To test the shear Alfvén wave we use the cold plasma dispersion relation obtained with the Hall term [the second term on the rhs of Eq. (11)] in the Ohm's law,[13]

$$\frac{\omega^2}{k_\parallel^2} = \left(1 - \frac{\omega}{\omega_{ci}}\right) v_A^2. \tag{26}$$

Figure 2 shows the simulation results for the frequency of a mode with $k_\parallel \rho_s = 0.0063$ and $k_\perp = 0$ in comparison with the frequency obtained from Eq. (26). Notice that as β_e decreases the finite ω/ω_{ci} correction in Eq. (26) becomes important. This is accurately captured by the Vlasov ion model.

B. ∇T_e driven drift Alfvén instability

We now allow an ETG in the x-direction, $\kappa_T = -T_e'/T_e > 0$. In order to derive a simple dispersion relation we assume ions are cold, $T_i = 0$. Assuming $\mathbf{E}_1 \sim \exp(i\mathbf{k}\cdot\mathbf{x} - i\omega t)$, etc., Eqs. (1), (10), and (11) and the linearized electron drift kinetic equation then lead to the following dispersion relation:

$$\begin{vmatrix} 1-\frac{i}{\omega\beta_e}k_xk_y-\frac{1}{D_i}+ik_xP_1 & \frac{i}{\omega\beta_e}(k_x^2+k_\parallel^2)-\frac{i\omega}{D_i}+ik_xP_2 & -\frac{i}{\omega\beta_e}k_\parallel k_y+ik_xP_3 \\ -\frac{i}{\omega\beta_e}(k_y^2+k_\parallel^2)+\frac{i\omega}{D_i}+ik_yP_1 & 1+\frac{i}{\omega\beta_e}k_xk_y-\frac{1}{D_i}+ik_yP_2 & \frac{i}{\omega\beta_e}k_\parallel k_x+ik_yP_3 \\ ik_\parallel S_1-\frac{m_e}{m_i}\frac{1}{\beta_e}k_\parallel k_x & ik_\parallel S_2+\kappa_T\frac{k_\parallel}{\omega}-\frac{m_e}{m_i}\frac{1}{\beta_e}k_\parallel k_y & 1+ik_\parallel S_3-\kappa_T\frac{k_y}{\omega}+\frac{m_e}{m_i}\frac{1}{\beta_e}k_\perp^2 \end{vmatrix}=0, \tag{27}$$

where the terms containing $D_i=-m_i^2\omega^2+q^2B_0^2$ come from the cold ion response. The parallel electron pressure is given by $\delta p_{\parallel e}=S_1E_{1x}+S_2E_{1y}+S_3E_{1\parallel}$ with

$$S_1=-m_ek_yI_2,$$

$$S_2=im_e\left[-\frac{1}{2}\kappa_TI_2+\frac{1}{2}m_e\kappa_TI_4-\frac{k_\parallel}{\omega}\left(-\frac{1}{2}\kappa_TI_3+\frac{1}{2}m_e\kappa_TI_5\right)-ik_xI_2\right], \tag{28}$$

$$S_3=im_e\left[\frac{k_y}{\omega}\left(-\kappa_TI_3/2+\frac{1}{2}m_e\kappa_TI_5\right)-I_3\right],$$

and the perpendicular electron pressure is given by $\delta p_{\perp e}=P_1E_{1x}+P_2E_{1y}+P_3E_{1\parallel}$ with

$$P_1=-2k_yI_0,$$

$$P_2=2i\left[\frac{1}{2}\kappa_TI_0+\frac{1}{2}m_e\kappa_TI_2-\frac{k_\parallel}{\omega}\left(\frac{1}{2}\kappa_TI_1+\frac{1}{2}m_e\kappa_TI_3\right)-ik_xI_0\right], \tag{29}$$

$$P_3=2i\left[\frac{k_\parallel}{\omega}\left(\frac{1}{2}\kappa_TI_1+\frac{1}{2}m_e\kappa_TI_3\right)-I_1\right],$$

and I_n is defined by

$$I_n=\int\frac{v_\parallel^n}{\omega-k_\parallel v_\parallel}\frac{1}{\sqrt{2\pi}v_T}e^{-v_\parallel^2/2v_T^2}dv_\parallel. \tag{30}$$

It is of interest to compare the solution of the dispersion relation, Eq. (27), with that from the gyrokinetic ions using $A_\parallel$ and ϕ as the field model.[14] Figures 3 and 4 show the frequency and growth rate of the drift Alfvén instabilities. The mode has $k_y\rho_s=3.5$, $k_x=0$, and $k_\parallel\rho_s=0.002\,84$. The ETG is $\kappa_T\rho_s=0.1$. The mode frequency obtained from the $A_\parallel/\phi$ model agrees very well with that obtained from Eq. (27) if the electron pressure $\delta p_{\perp e}$ is discarded in the perpendicular Ohm's equation, Eq. (11) [i.e., if P_i are set to zero in Eq. (27)]. The effect of $\delta p_{\perp e}$ becomes increasingly important as β_e increases. This effect is missing in the $A_\parallel/\phi$ model, in which only the parallel component of the Ampere's equation, Eq. (2), is solved for $A_\parallel$, and the electron diamagnetic current due to $\nabla\delta p_{\perp e}$ simply does not appear.

We identify this instability as the drift Alfvén instability because when there is no ETG the instability becomes the kinetic Alfvén wave.[15] If the ion response is dropped [i.e., dropping terms containing D_i in Eq. (27)], the mode becomes the whistler mode with much larger growth rate.

The simulation results for $\delta p_{\perp e}=0$ are also shown in

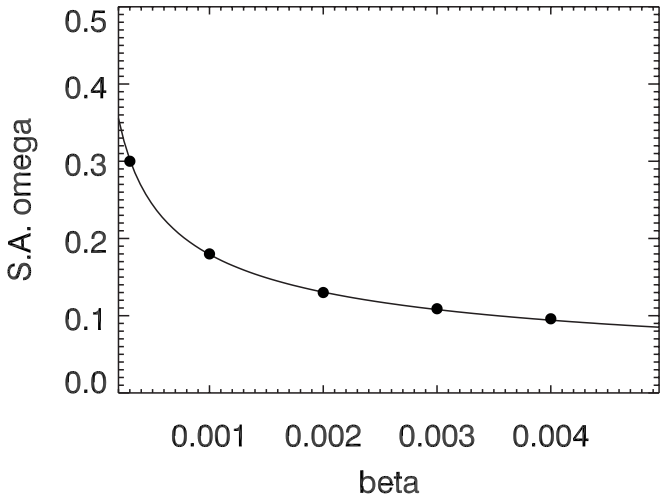

FIG. 2. Simulated shear Alfvén wave frequencies vs β_e (points) compared with the dispersion relation (solid line).

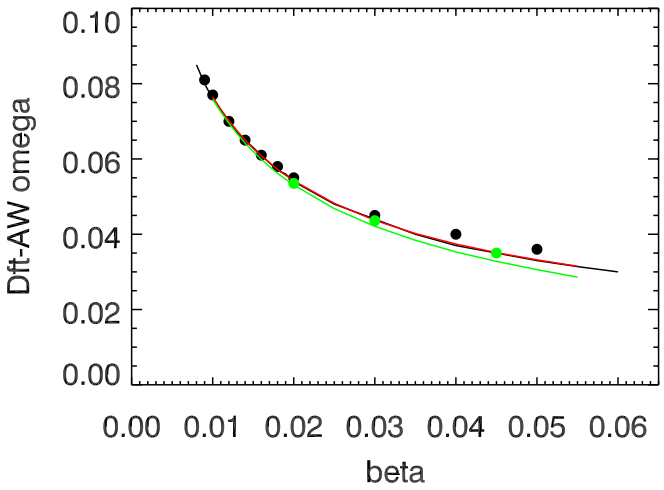

FIG. 3. (Color online) Drift Alfvén wave frequencies vs β_e for $k_x=0$, $k_\perp\rho_s=3.5$, and $k_\parallel\rho_s=0.002\,84$. The black line is obtained from the dispersion relation, Eq. (27), with the perturbed electron perpendicular pressure set to zero. The light gray line (green online) is obtained from the same dispersion relation but with the perturbed electron perpendicular pressure. The dark gray line (red online) is obtained from the dispersion relation for the $A_\parallel/\phi$ field model. The data points are from simulations: black with $\delta p_{\perp e}=0$ and green with $\delta p_{\perp e}\neq 0$.

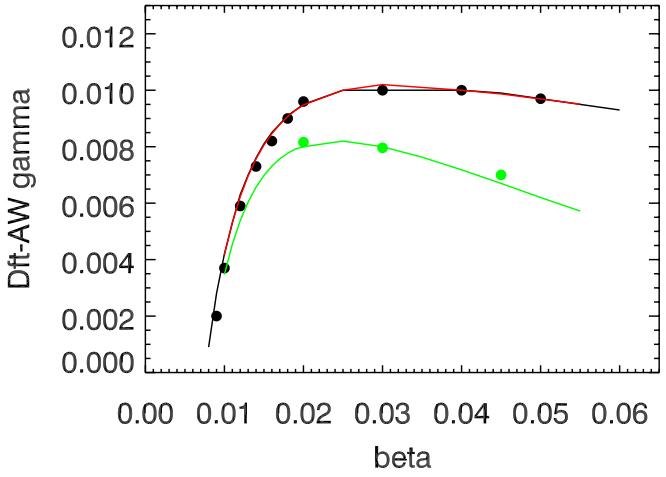

FIG. 4. (Color online) Same as in Fig. 3 but for the mode growth rates.

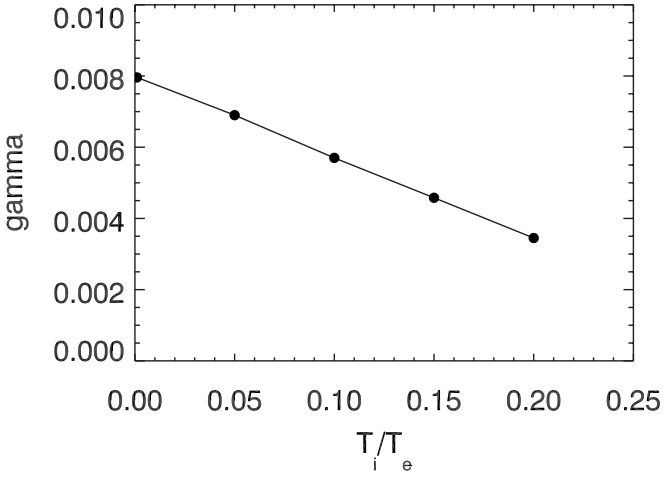

FIG. 6. The same as in Fig. 5 but for the mode growth rates.

Figs. 3 and 4. These simulations use the following parameters: the number of grids is $(n_x,n_y,n_\parallel)=(4,64,64)$, 64 particles per grid cell per species, time step $\omega_{ci}\Delta t=0.05$. A small but finite $T_i/T_e=0.001$ is used because the ion weight equation in the δf method is singular at $T_i=0$. The simulation results for $\delta p_{\perp e}\neq 0$ (shown in green dots) also agree with the dispersion relation.

As the ion temperature increases we expect the finite ion Larmor radius to have a stabilizing effect on the drift Alfvén instability. This is indeed observed, as shown in Figs. 5 and 6. For these simulations $\beta_e=0.003$ and $\delta p_{\perp e}$ is retained.

C. Ion acoustic waves

In deriving the generalized Ohm's equation, Eq. (10), the ion term in Eq. (9) has been neglected because it is smaller than the electron terms by $\sim m_e/m_i$. However, the ion term is needed for describing the IAWs, for which $k_\perp=0$, $\mathbf{B}_1=0$, and the parallel Ohm's equation is the only nontrivial field equation (recall that the quasineutrality condition $Zn_i=n_e$ is not used in the model). With the ion terms added Eq. (12) becomes (with $\mathbf{B}_1=0$)

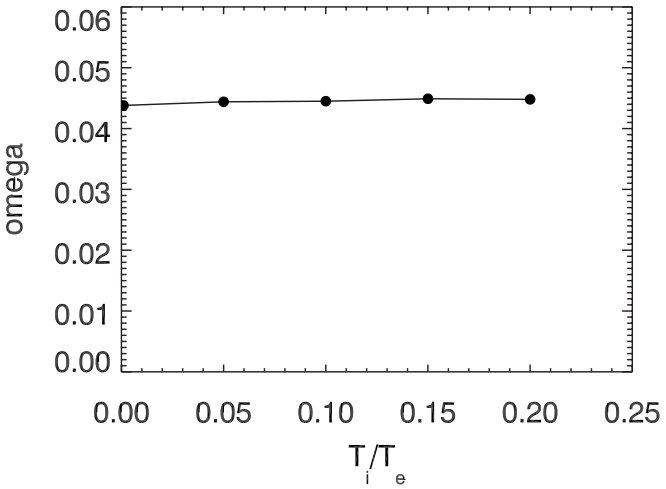

FIG. 5. The drift Alfvén mode frequencies vs ion temperature for the same mode as in Fig. 3 but with $\beta_e=0.003$.

$$\left(1+\frac{m_e}{m_i}\right)E_{1\parallel}=-\nabla_\parallel\delta p_{\parallel e}+\frac{m_e}{m_i}\nabla_\parallel\delta p_{\parallel i}. \tag{31}$$

It is difficult to observe the IAWs in simulations that solve Eq. (31). The reason is clear. In the cold ion limit $\delta p_{\parallel i}=0$, the ion inertia effect appears as the small m_e/m_i term on the lhs. If the numerical error in $\delta p_{\parallel e}$ is comparable to this small term, the IAW cannot be observed. This can also be understood by considering the IAW dispersion relation. To the zeroth order in m_e/m_i the electrons behave adiabatically in an IAW, $\delta n_e=en_0\phi/T_e$, and the electron pressure response is given by $\delta p_{\parallel e}=en_0\phi$. Therefore the $O(1)$ terms in Eq. (31) vanish identically. The IAW dispersion relation appears only through the $O(m_e/m_i)$ terms in Eq. (31).

One can force the essential IAW dispersion relation to appear through the zeroth order terms (in m_e/m_i) in Eq. (31) by replacing $\delta p_{\parallel e}$ with

$$\delta p'_{\parallel e}=\delta p_{\parallel e}+T_e(Z\delta n_i-\delta n_e). \tag{32}$$

The zeroth order term of Eq. (31) is now simply $\delta n_i-\delta n_e=0$ (assuming $Z=1$), which yields for cold ions the IAW dispersion relation $\omega=k_\parallel\sqrt{T_e/m_i}$.

The direct consequence of the Ampere's equation, Eq. (2), is that the current is divergence-free $\nabla\cdot\mathbf{j}=0$. The net charge $Z\delta n_i-\delta n_e$ can be nonzero but does not vary in time. It is straightforward to show that use of $\delta p'_{\parallel e}$ leads to a rapid oscillation $\omega\sim k_\parallel\sqrt{T_e/m_e}$ of the net charge. Although this unphysical oscillation is numerically stable in the implicit scheme, it causes the simulation more noisy. Charge neutrality can be enforced by removing the net charge in each spatial cell from the electron weights. Denoted by Δw the difference between the average electron weights and the average ion weights in each spatial cell, we adjust the weights of those electrons inside the cell according to

$$w'=w-\delta\Delta w \tag{33}$$

at the end of each time step. Typically $\delta=0.05$ is sufficient for suppressing the fast oscillations. Note that this procedure has no effect on physical modes, which satisfy quasineutrality.

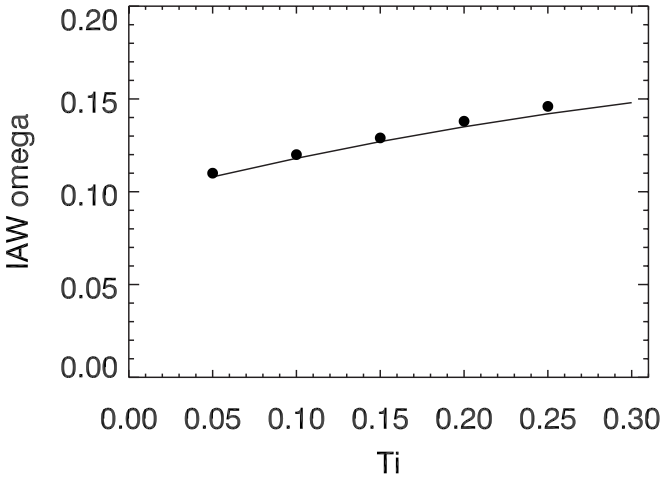

FIG. 7. IAW frequency vs ion-electron temperature ratio for $k_\parallel \rho_s = 0.1$. The line is from the dispersion relation.

Figures 7 and 8 show the simulation results of the $k_\parallel \rho_s = 0.1$ IAW using the above scheme with $\delta = 0.05$. As the ion temperature varies, both the real frequency and the damping rate agree well with the IAW dispersion relation [not Eq. (27)].

V. DISCUSSION

The hybrid simulation model developed in this paper is motivated by recent topics in gyrokinetic turbulence simulations. Questions have been raised concerning the adequacy or efficiency of simulations of both long and short wavelength modes. In the long wavelength case, Parra and Catto[16] showed that the use of gyrokinetic Poisson equation to determine the zonal flow modes on the macroscopic scale $k_r a \sim 1$ (a is the minor radius) violates the gyrokinetic ordering. Present gyrokinetic simulations crucially rely on the fact that the ion polarization density appears explicitly in the Poisson equation,[5] which otherwise cannot be used to determine the potential ϕ in the quasineutral case. Parra and Catto noticed that the polarization density in the long wavelength regime scales as $\sim k_\perp^2 \phi$. In a gyrokinetic ordering where $\varepsilon = \rho_i / a$ is used as the smallness parameter and $e\phi / T_e \sim \varepsilon$, the polarization density becomes second order in ε. Since in present gyrokinetic simulations δf, hence the perturbed ion density is solved only to first order accuracy in ε, solving the gyrokinetic Poisson equation for $k_\perp a \sim 1$ zonal flow modes does not make sense.

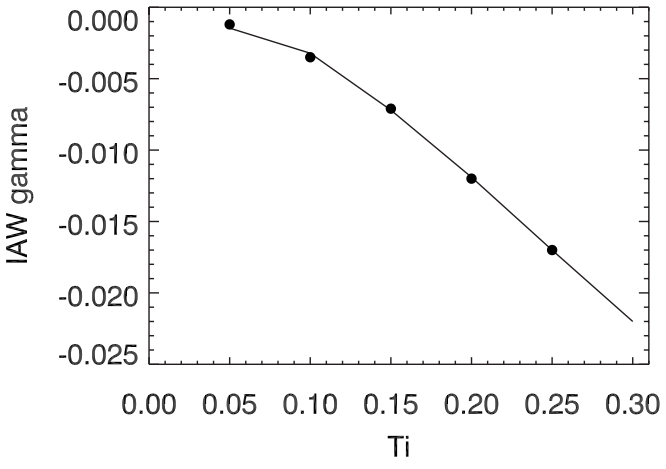

FIG. 8. The same as in Fig. 7 but for the IAW damping rate.

Another difficulty with $k_\perp \rho_i \ll 1$ modes in gyrokinetic simulations arises from the Ampere's equation for the vector potential $A_\parallel$. We recall that in order to avoid numerically evaluating the inductive parallel electric field $\partial A_\parallel / \partial t$, the particle canonical momentum $p_\parallel = v_\parallel + (q/m) A_\parallel$ is used as a coordinate. This renders the Ampere's equation into the following form:

$$\left(-\nabla_\perp^2 + \frac{\omega_{pe}^2}{c^2} \right) A_\parallel = \mu_0 \delta j_\parallel, \tag{34}$$

which causes the "cancellation problem." For typical wavelength of interest, the second term on the lhs is orders of magnitude larger than the first term, requiring very accurate calculation of the rhs to ensure proper cancellation. This problem is solved for $k_\perp \rho_i > 0.1$.[12] Longer wavelength modes are usually stable or weakly unstable, making independent verification of the Ampere solver difficult. In any case, adequate cancellation requires smaller grid sizes and time step for sufficient numerical accuracy, hence using the $p_\parallel$ formulation and solving Eq. (34) for long wavelength modes require finer grids. This trend is counterintuitive, since one expects to be able to use fewer grids to resolve long wavelength modes.

For short wavelength modes such as the ETG modes, present PIC simulations are electrostatic and typically assume an adiabatic ion response. Simulations with continuum codes, however, indicate that the nonadiabatic response of the ions is important.[17] To capture this effect in PIC simulation requires careful evaluation of the gyroaveraged electric field. Such averaging in ITG-like simulations is done with the four-point averaging scheme,[18] but for the much shorter wavelength ETG modes more points along the gyroring are needed. On the other hand, for a Vlasov model the computational cost is not affected by the presence of short wavelength modes, since one needs to sample many points along the gyro-orbit in any case.

Turbulent transport is a complex process involving multiple time and spatial scales. The gyrokinetic formalism aims to analytically eliminate the fast scale (e.g., scales associated with the compressional Alfvén waves) from the equations via a perturbation approach. Modern gyrokinetic theory provides a systematic procedure for carrying out such a perturbation analysis to arbitrary order. In practice, however, perturbative approach is rarely carried to beyond the first order. The number of terms resulting from perturbative analysis increases rapidly as one moves to higher order. In cases where accuracy is the primary concern, as for instance in the plasma edge where the equilibrium scale length of the density is not well separated from the ion Larmor radius or the fluctuation amplitude is large (say $e\phi / T_e \geq 0.1$), pursuing the gyrokinetic formalism beyond the first order could be important but is unappealing. On the other hand, fast time scales associated with the compressional Alfvén waves can be eliminated us-

ing numerical techniques that solve the primitive equation, the Vlasov equation, directly. The problem of the validity of perturbation analysis does not arise. The shift from a gyrokinetic model to the Vlasov model advocated in this paper can be viewed as such a step.

In this paper we demonstrate that an implicit scheme can indeed eliminate the fast waves. A simple finite-difference scheme [e.g., Eq. (18)] that is not centered in time is used. More efficient integration scheme can be used. Since the time scale of interest is much longer than the ion gyroperiod, the technique of orbit averaging[19] can be used for ions. The field equations, Eqs. (10) and (11), can be solved each macrostep (say, with $\Omega\Delta t \sim 1$). The ion motion (and in δf method, the increment to the ion weights) over such a macrostep can be computed by integrating the ion equations over many time substeps. We do not attempt to explore this issue further here, as this and other numerical details will arise when the hybrid model is implemented in a toroidal geometry and better explored in that context. Without going into details, however, one can anticipate that solving the discretized field equations, Eqs. (19) and (20), will be a primary concern in a toroidal geometry. The parallelization scheme of the entire simulation must to a large extent be determined by considerations of an efficient parallelization of the field solver.

APPENDIX: GYROKINETIC ELECTRONS

The hybrid simulation model presented in this paper uses $\mathbf{E}_1$ and $\mathbf{B}_1$ directly. The electric potential ϕ and the vector potential $\mathbf{A}$ are not needed. Gyrokinetic equations, on the other hand, are usually derived using the latter field variables in order to take advantage of the explicit ordering between the two components of $\mathbf{E}_1 = -\nabla\phi - \partial\mathbf{A}/\partial t$,

$$\frac{\partial \mathbf{A}}{\partial t} \sim \varepsilon_\delta \nabla_\perp \phi. \tag{A1}$$

Since the implicit scheme of Sec. III is based on solving for $\mathbf{E}_1$ and $\mathbf{B}_1$, it is necessary to write the gyrokinetic equation in terms of $\mathbf{E}_1$ and $\mathbf{B}_1$. The Frieman–Chen gyrokinetic equation[8] written in the velocity coordinates $(\epsilon = v^2/2, \mu)$ and assuming isotropy $(\partial F_0/\partial\mu = 0)$ is

$$\hat{L}_g \delta H_0 \equiv \left(\frac{\partial}{\partial t} + v_\parallel \mathbf{b}\cdot\nabla + \mathbf{v}_D\cdot\nabla\right)\delta H_0 = -\frac{q}{m}(S_L + \langle R_{NL}\rangle), \tag{A2}$$

where δH_0 is related to the perturbed distribution δF through

$$\delta F = \frac{q}{m}\phi\frac{\partial F_0}{\partial \epsilon} + \delta H_0, \tag{A3}$$

and

$$S_L = \frac{\partial}{\partial t}\langle \phi - \mathbf{v}\cdot\mathbf{A}\rangle \frac{\partial F_0}{\partial \epsilon} - \nabla\langle \phi - \mathbf{v}\cdot\mathbf{A}\rangle \times \frac{\mathbf{b}}{\Omega}\cdot\nabla F_0, \tag{A4}$$

$$\langle R_{NL}\rangle = -\nabla\langle \phi - \mathbf{v}\cdot\mathbf{A}\rangle \times \frac{\mathbf{b}}{\Omega}\cdot\nabla\delta H_0. \tag{A5}$$

Note that although δH_0 is gyrophase independent, δF depends on the gyrophase through ϕ. We define

$$\delta f = \frac{q}{m}\langle\phi\rangle\frac{\partial F_0}{\partial\epsilon} + \delta H_0, \tag{A6}$$

so that

$$\delta F = \frac{q}{m}(\phi - \langle\phi\rangle)\frac{\partial F_0}{\partial\epsilon} + \delta f. \tag{A7}$$

The gyrokinetic equation for δf is obtained from Eq. (A2),

$$\hat{L}_g \delta f = -\nabla\langle \phi - \mathbf{v}\cdot\mathbf{A}\rangle \times \frac{\mathbf{b}}{\Omega}\cdot\nabla F_0 + \frac{1}{m}\dot{\epsilon}\frac{\partial F_0}{\partial\epsilon} + \frac{q}{m}\nabla\langle \phi - \mathbf{v}\cdot\mathbf{A}\rangle \times \frac{\mathbf{b}}{\Omega}\cdot\nabla\delta f, \tag{A8}$$

with

$$\dot{\epsilon} = q\left(v_\parallel \mathbf{b} + \mathbf{v}_D + \frac{q}{m}\nabla\langle\mathbf{v}\cdot\mathbf{A}\rangle \times \frac{\mathbf{b}}{\Omega}\right)\cdot\nabla\langle\phi\rangle + \frac{\partial}{\partial t}\langle\mathbf{v}\cdot\mathbf{A}\rangle. \tag{A9}$$

The notation $\dot{\epsilon}$ is appropriate because it is in fact the rate of change in the particle kinetic energy, $mv^2/2$. We can now write Eq. (A8) in terms of $\mathbf{E}_1$ and $\mathbf{B}_1$. Using

$$\langle \mathbf{v}_\perp\cdot\nabla\Psi\rangle = \frac{1}{2\pi}\oint \Omega\frac{\partial}{\partial\alpha}\Psi[\mathbf{R} + \boldsymbol{\rho}(\alpha)] = 0 \tag{A10}$$

(α is the gyroangle) for arbitrary scalar field Ψ, it is easy to show

$$\nabla\langle\mathbf{v}\cdot\mathbf{A}\rangle = \langle\mathbf{v}\times\mathbf{B}_1\rangle, \tag{A11}$$

so that the guiding center velocity containing $\langle\mathbf{v}\cdot\mathbf{A}\rangle$ becomes

$$\frac{q}{m}\nabla\langle\mathbf{v}\cdot\mathbf{A}\rangle \times \frac{\mathbf{b}}{\Omega} = v_\parallel\frac{\langle\mathbf{B}_{1\perp}\rangle}{B_0} - \frac{1}{B_0}\langle\mathbf{v}_\perp B_{1\parallel}\rangle. \tag{A12}$$

The term in $\dot{\epsilon}$ involving $\partial\mathbf{A}/\partial t$ is given by

$$\frac{\partial}{\partial t}\langle\mathbf{v}\cdot\mathbf{A}\rangle = v_\parallel\left\langle\frac{\partial A_\parallel}{\partial t}\right\rangle - \langle\mathbf{v}_\perp\cdot(\mathbf{E}_{1\perp} + \nabla_\perp\phi)\rangle = v_\parallel\left\langle\frac{\partial A_\parallel}{\partial t}\right\rangle - \langle\mathbf{v}_\perp\cdot\mathbf{E}_{1\perp}\rangle. \tag{A13}$$

Next we notice that $E_\parallel = -\nabla_\parallel\phi - \partial A_\parallel/\partial t$ and, in standard gyrokinetic ordering $\mathbf{E}_{1\perp} \approx \nabla_\perp\phi$, Eq. (A8) can be written as

$$\frac{D}{Dt}\delta f = -\left(\frac{1}{B_0}\langle\mathbf{E}_1\rangle\times\mathbf{b} + v_\parallel\frac{\langle\mathbf{B}_{1\perp}\rangle}{B_0}\right)\cdot\nabla F_0 + \frac{1}{m}\dot{\epsilon}\frac{\partial F_0}{\partial\epsilon}, \tag{A14}$$

where

$$\frac{D}{Dt} = \hat{L}_g + \left(\frac{1}{B_0}\langle\mathbf{E}_1\rangle\times\mathbf{b} + v_\parallel\frac{\langle\mathbf{B}_{1\perp}\rangle}{B_0}\right)\cdot\nabla \tag{A15}$$

and

$$\dot{\epsilon} = q\left(v_{\parallel}\mathbf{b} + \mathbf{v}_D + v_{\parallel}\frac{\langle \mathbf{B}_{1\perp}\rangle}{B_0}\right)\cdot\langle \mathbf{E}_1\rangle + q\langle \mathbf{v}_{\perp}\cdot\mathbf{E}_{1\perp}\rangle \tag{A16}$$

We now calculate the perturbed electron flow from the total perturbed electron distribution, Eq. (A7). The parallel flow from δf is computed as usual, i.e., by depositing particle parallel velocity along its gyroring. The perpendicular flow from δf is

$$\begin{aligned} n_0\mathbf{U}_D(\mathbf{x}) &= \int \mathbf{v}_{\perp}\delta f(\mathbf{x},\mathbf{v})d\mathbf{v} \\ &= \int \mathbf{v}_{\perp}\delta f(\mathbf{x}',\mathbf{v})\delta(\mathbf{x}-\mathbf{x}')d\mathbf{x}'d\mathbf{v} \\ &= \int \mathbf{v}_{\perp}(\mathbf{R}',\epsilon,\mu,\alpha)\delta f(\mathbf{R}',\epsilon,\mu)\delta(\mathbf{x}-\mathbf{R}' \\ &\quad -\boldsymbol{\rho})Jd\mathbf{R}'d\epsilon d\mu d\alpha \\ &= \int \mathbf{v}_{\perp}(\mathbf{x}-\boldsymbol{\rho},\epsilon,\mu,\alpha)\delta f(\mathbf{x}-\boldsymbol{\rho},\epsilon,\mu)Jd\mathbf{R}'d\epsilon d\mu d\alpha, \end{aligned} \tag{A17}$$

where $d\mathbf{v}=Jd\epsilon d\mu d\alpha$. To the first order in the gyrokinetic ordering parameter $\varepsilon\sim\rho/L_B\sim e\phi/T$ (L_B is the equilibrium magnetic field scale length), the dependence of the scalar quantities $v_{\perp}$ and ρ on the gyrophase can be neglected,

$$\mathbf{v}_{\perp} = v_{\perp}(\hat{\mathbf{x}}\cos\alpha - \hat{\mathbf{y}}\sin\alpha),$$

$$\boldsymbol{\rho} = \frac{v_{\perp}}{\Omega}(\hat{\mathbf{x}}\sin\alpha + \hat{\mathbf{y}}\cos\alpha),$$

where $v_{\perp}$ and Ω on the rhs are evaluated at $(\mathbf{x},\epsilon,\mu)$. We now expand $\delta f(\mathbf{x}-\boldsymbol{\rho},\epsilon,\mu)$ around $\mathbf{x}$. Suppressing the dependence on ϵ and μ,

$$\delta f(\mathbf{x}-\boldsymbol{\rho}) = \delta f(\mathbf{x}) - \boldsymbol{\rho}\cdot\nabla\delta f + \tfrac{1}{2}\boldsymbol{\rho}\boldsymbol{\rho}:\nabla\nabla\delta f + O(\rho^3). \tag{A18}$$

Upon substitution into Eq. (A17) and integration over velocity, the first term vanishes and the second term leads to the second term on the rhs of Eq. (6), i.e., the electron diamagnetic flow associated with the perturbed pressure. The contribution of the third term in Eq. (A18) to $\mathbf{U}_D$ is

$$\frac{1}{2e^2B^2}\nabla_{\perp}^2\int \mathbf{v}_{\perp}\frac{1}{2}mv_{\perp}^2\delta f d\mathbf{v}, \tag{A19}$$

which can in general be neglected for $k_{\perp}\rho<1$. In the strongly gyrokinetic regime $k_{\perp}\rho\sim 1$, Eq. (A17) cannot be further reduced and $\mathbf{U}_D$ can in principle be calculated by depositing the vector $\mathbf{v}_{\perp}$ along the gyroring.

Contribution to electron flow from the first term in Eq. (A7) is

$$n_0\mathbf{U}_E(\mathbf{x}) = \frac{\mathbf{q}}{\mathbf{m}}\int \mathbf{v}[\phi(\mathbf{x}) - \langle\phi\rangle(\mathbf{x}-\boldsymbol{\rho},\epsilon,\mu)]\frac{\partial F_0}{\partial\epsilon}J\mathbf{d}\epsilon\mathbf{d}\mu\mathbf{d}\alpha. \tag{A20}$$

To express $n_0\mathbf{U}_E$ in terms of $\mathbf{E}_1$ we assume an eikonal form for ϕ, $\phi(\mathbf{x})=\phi_k e^{i\mathbf{k}\cdot\mathbf{x}}$, so that $\mathbf{E}_{k\perp}=-i\mathbf{k}_{\perp}\phi_k e^{i\mathbf{k}\cdot\mathbf{x}}$. Assuming F_0 is Maxwellian and carrying out the velocity integral,

$$n_0\mathbf{U}_E = n_0\frac{h}{B_0}\mathbf{E}_{k\perp}\times\mathbf{b} \tag{A21}$$

with $b=k_{\perp}^2v_T^2/\Omega^2$ and

$$h(b) = -\frac{1}{b^2}\int_0^{\infty} e^{-x^2/2b}J_0(b)J_0'(b)x^2dx. \tag{A22}$$

In the limit of small $k\rho\ll 1$ the factor $h(b)$ becomes unity, so that $n_0\mathbf{U}_E$ becomes the total guiding center $\mathbf{E}\times\mathbf{B}$ flow, as in Eq. (6).

[1] E. V. Belova, N. N. Gorelenkov, and C. Z. Cheng, Phys. Plasmas **10**, 3240 (2003).
[2] T. S. Hahm, Phys. Plasmas **3**, 4658 (1996).
[3] H. Qin, R. H. Cohen, W. M. Nevins, and X. Q. Xu, Phys. Plasmas **14**, 056110 (2007).
[4] Y. Chen and S. E. Parker, J. Comput. Phys. **220**, 839 (2007).
[5] W. W. Lee, Phys. Fluids **26**, 556 (1983).
[6] A. J. Brizard and T. S. Hahm, Rev. Mod. Phys. **79**, 421 (2007).
[7] H. Qin and W. M. Tang, Phys. Plasmas **11**, 1052 (2004).
[8] E. Frieman and L. Chen, Phys. Fluids **25**, 502 (1982).
[9] M. Tanaka, J. Comput. Phys. **107**, 124 (1993).
[10] Y. Lin, X. Wang, Z. Lin, and L. Chen, Plasma Phys. Controlled Fusion **47**, 657 (2005).
[11] D. C. Barnes, J. Cheng, and S. E. Parker, Phys. Plasmas **15**, 055702 (2008).
[12] Y. Chen and S. E. Parker, J. Comput. Phys. **189**, 463 (2003).
[13] R. Cross, *An Introduction to Alfvén Waves* (Adam Hilger, Philadelphia, 1988).
[14] Y. Chen and S. E. Parker, Phys. Plasmas **8**, 2095 (2001).
[15] A. Hasegawa and L. Chen, Phys. Rev. Lett. **35**, 370 (1975).
[16] F. I. Parra and P. J. Catto, Plasma Phys. Controlled Fusion **50**, 065014 (2008).
[17] J. Candy and R. E. Waltz, *21st IAEA Fusion Energy Conference* (International Atomic Energy Agency, Vienna, 2006).
[18] W. Lee, J. Comput. Phys. **72**, 243 (1987).
[19] B. I. Cohen, T. A. Brengle, D. B. Conley, and R. P. Freis, J. Comput. Phys. **38**, 45 (1980).